

Assembly of a freeform off-axis optical system employing three φ -polynomial Zernike mirrors

Kyle Fuerschbach,^{1,*} Gregg E. Davis,² Kevin P. Thompson,^{3,1} and Jannick P. Rolland¹

¹The Institute of Optics, University of Rochester, 275 Hutchison Road, Rochester, New York 14627, USA

²II-VI Infrared, 375 Saxonburg Boulevard, Saxonburg, Pennsylvania 16056, USA

³Synopsys Inc., 3 Graywood Lane, Pittsford, New York 14534, USA

*Corresponding author: fuerschb@optics.rochester.edu

Received March 5, 2014; accepted April 3, 2014;
posted April 10, 2014 (Doc. ID 207685); published May 8, 2014

We report on the assembly of an off-axis reflective imaging system employing freeform, φ -polynomial optical surfaces. The sensitivity of the system to manufacturing errors is studied for both a passive and active alignment approach. The as-built system maintains diffraction-limited performance in the long-wave infrared. © 2014 Optical Society of America

OCIS codes: (080.4228) Nonspherical mirror surfaces; (220.1920) Diamond machining; (220.1140) Alignment.
<http://dx.doi.org/10.1364/OL.39.002896>

Freeform optical surfaces open a new space for optical design, as they can be used to correct the aberrations induced by a non-inline, tilted, or decentered optical system [1,2]. New fabrication and assembly challenges arise when building an optical system of this type because conventional methods of fabrication must be abandoned to enable these new optical design forms. Moreover, when assembling an optical system of this type, the mounting and fiducialization of the optical surfaces become critical because the optical surfaces must now be oriented in a particular manner and constrained in all six degrees of freedom [3].

In this Letter, the mechanical design of a freeform optical system is presented, and the sensitivity of the optical system to fabrication errors is evaluated. Also, the as-built system and its optical performance are presented. The freeform optical system comes from a recent design targeted at an unobscured, F/1.9, 10° full field of view (FOV) long-wave infrared (LWIR) imager that employs three freeform, φ -polynomial (Zernike) mirrors and couples to an uncooled microbolometer [2]. A layout of the nominal optical design is shown in Fig. 1(a). The RMS wavefront error (RMSWFE) of the nominal design is less than 0.02 λ at 10 μm over a 10° diagonal full FOV.

The housing structure of the three-mirror system is displayed in Fig. 1(b) and was developed in collaboration with II-VI Infrared. It is constructed from an aluminum block with the faces of the block machined to the required tilt angle for each mirror. The mirrors are designed to be back-surface mounted so an adaptor plate is used to couple the mirror to its corresponding face. Steel dowel pins are used to position the mirror correctly within the mechanical housing. These dowel pins provide a good mechanical datum to the optical surface because during the fabrication process they register the optical surface to a tooling plate with a reference flat that is tried to the diamond turning machine. In total, there are two mechanical connections for each mirror subassembly. The first connection is between the optical surface and the adaptor plate, and the second connection is between the adaptor plate and the housing face. At each connection, three diamond turned raised pads are used as the mounting interface to provide a quasi-kinematic

condition when the two surfaces are mated together. The pads also compensate for any errors in the mirror thicknesses, as they are machined based on measurements of the fabricated housing and mirror components. In total, the pin connections constrain the x decenter, y decenter, and clocking angle of the optical surface with screws providing preload, thus constraining any in-plane movement. Holes are bored into the structure to ensure that light passes through the housing without vignetting.

As is the case with any piece of hardware, there is some tolerance on how well the mirrors can be positioned in the housing relative to their nominal value. The key is to ensure that within the manufacturing tolerances, the as-built optical system remains diffraction limited. Also, the assembly method of the optical system may impact the manufacturing tolerances. If the optical system is to be passively aligned, that is, no adjustments are made with the exception of focus, the manufacturing tolerances will have to be tighter. If the system is to be actively aligned, that is, a compensator is used to restore the optical performance after assembly, the assessment of the performance during alignment is important and the mechanical complexity of the housing will have to increase because a degree of freedom must now be made adjustable. In this Letter, both approaches are explored and implemented in the as-built optical system and the achievable optical performance is presented for each approach.

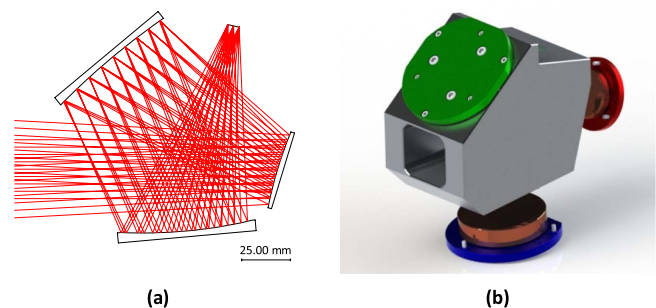


Fig. 1. (a) Optical layout of the freeform LWIR imaging system optimized with φ -polynomial surfaces and (b) layout of the housing structure of the optical system.

For this system in a passive alignment approach, the three mirrors must be constrained in their x and y translation as well as tip, tilt, and clocking angle. There are also two vertex spacings that must be held between the three mirrors. The spacing between the tertiary mirror and focal plane is used as a focus adjustment after assembly. The focus compensation is performed by shimming the detector in $12.5\ \mu\text{m}$ steps and determining through an optical assessment the shim that provides the best performance. The detector must also be held in tip and tilt relative to the housing, and there is a separate tip and tilt tolerance for the focal plane relative to the mounting fixtures on the detector. In total, there are 21 positioning tolerances to consider for this assembly.

To check the sensitivity of the optical housing to manufacturing errors, each tolerance is perturbed a specified amount and the change in the RMSWFE after focus compensation is recorded for various field points throughout the FOV. Once each tolerance and its resulting change in performance is computed, the total change in performance for each field can be computed as the root sum square (RSS) of all the tolerances [4]. The results of this analysis are displayed in Table 1, where the change in RMSWFE is displayed for each tolerance at two field points: on-axis ($0^\circ, 0^\circ$) and the most sensitive field ($4^\circ, 3^\circ$). Looking at the tolerances on a term-by-term basis,

Table 1. Sensitivity Analysis of the Three Mirror Optical System^a

Item	Tolerance	Δ RMSWFE Field: ($0^\circ, 0^\circ$)	Δ RMSWFE Field: ($4^\circ, 3^\circ$)
<i>Primary Mirror</i>			
x decenter	$\pm 50\ \mu\text{m}$	0.002	0.002
y decenter	$\pm 50\ \mu\text{m}$	0.006	0.005
Tip	$\pm 0.017^\circ$	0.003	0.001
Tilt	$\pm 0.017^\circ$	0.001	0.001
Clocking	$\pm 0.1^\circ$	0.000	0.000
Vertex spacing	$\pm 50\ \mu\text{m}$	0.001	0.001
<i>Secondary Mirror</i>			
x decenter	$\pm 50\ \mu\text{m}$	0.003	0.004
y decenter	$\pm 50\ \mu\text{m}$	0.010	0.006
Tip	$\pm 0.017^\circ$	0.023	0.018
Tilt	$\pm 0.017^\circ$	0.014	0.015
Clocking	$\pm 0.1^\circ$	0.003	0.004
Vertex spacing	$\pm 50\ \mu\text{m}$	0.000	0.000
<i>Tertiary Mirror</i>			
x decenter	$\pm 50\ \mu\text{m}$	0.000	0.000
y decenter	$\pm 50\ \mu\text{m}$	0.003	0.003
Tip	$\pm 0.017^\circ$	0.013	0.008
Tilt	$\pm 0.017^\circ$	0.006	0.007
Clocking	$\pm 0.1^\circ$	0.031	0.031
<i>Detector</i>			
Tip	$\pm 0.017^\circ$	0.000	0.000
Tilt	$\pm 0.017^\circ$	0.000	0.000
<i>Focal Plane</i>			
Tip	$\pm 0.56^\circ$	0.000	0.015
Tilt	$\pm 0.56^\circ$	0.000	0.023
RSS		0.045^b	0.050
Nominal		0.011	0.010
Predicted as-built		0.056	0.060

^aThe RMS wavefront error values are in waves at the central operating wavelength of $10\ \mu\text{m}$.

^bBold values represent the overall system RMS wavefront error: RSS, nominal, and as-built.

the primary contributors to the overall loss in performance are the tip/tilt tolerances on the secondary mirror, tertiary mirror, and focal plane. With all the tolerances considered, the as-built RMSWFE is found to be roughly 0.056λ for the ($0^\circ, 0^\circ$) field and 0.060λ for the ($4^\circ, 3^\circ$) field, both of which are within the diffraction limit of 0.07λ . Therefore, the tolerances selected in Table 1 are sufficient for meeting the performance specification in the LWIR; however, if the design is to be pushed to shorter wavelength regimes, active alignment will be beneficial.

In an active alignment approach, the RMSWFE at a given field point is no longer used as the performance metric because it does not provide any information on which aberration contributions are limiting the performance and how they vary throughout the FOV. If the degrees of freedom of the system are perturbed a known amount and now the FRINGE Zernike aberration contributions are monitored throughout the FOV using the full field display (FFD), which plots the magnitude and orientation of the Zernike polynomials on a term-by-term basis over a two dimensional grid of field points, additional insight can be gained on alignment strategies, as well as which degrees of freedom are going to work best as compensators. From the results of the sensitivity analysis in Table 1, it is seen that for the optical system, in general, there is a greater loss in performance when the mirror components are tilted versus decentered, so

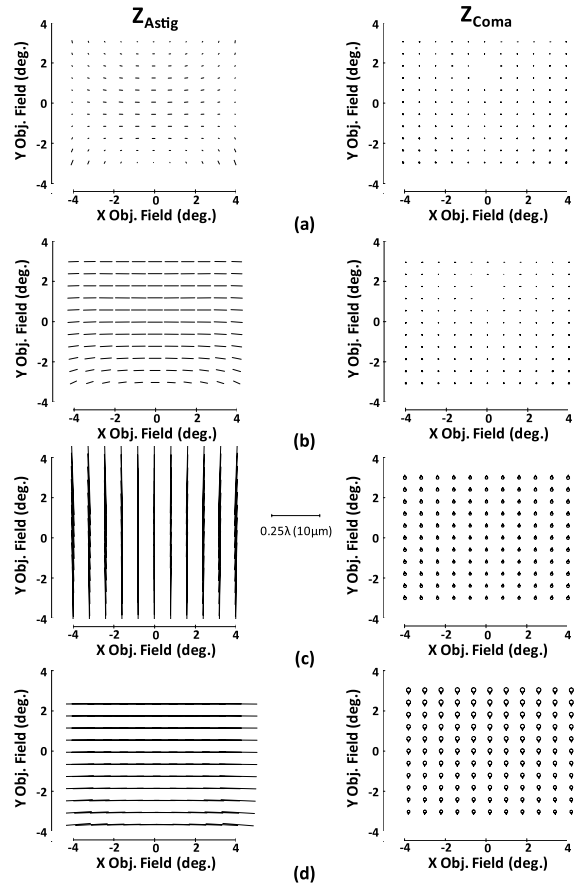


Fig. 2. Astigmatism ($Z_{5/6}$) and coma ($Z_{7/8}$) Zernike aberration FFDs over an $8^\circ \times 6^\circ$ full FOV for the (a) nominal system and with 0.1° tilt of the (b) primary, (c) secondary, and (d) tertiary mirror surfaces.

an effective compensator will be the mirror tilt. To see the aberration effect of the mirror tilt, Figs. 2(a)–2(d) display the FFDs for FRINGE Zernike astigmatism ($Z5/6$) and Zernike coma ($Z7/8$) for the nominal optical system, shown in Fig. 2(a), and for the case where the mirrors are individually tilted $+0.1^\circ$ in the YZ plane, shown in Figs. 2(b)–2(d). For each case, the primary aberration component induced is field constant astigmatism. Some field constant coma is induced, though its magnitude is about 10 times less than that of the astigmatism.

From the results of Fig. 2, several conclusions can be drawn. First, since field constant astigmatism is primarily induced when the telescope is misaligned, during alignment only one field point needs to be monitored to get a good representation of how the other field points are behaving. Second, for the same tilt of the three mirrors, the secondary is most sensitive to perturbation. Consequently, this mirror may make the most effective compensator because a small perturbation of the mirror will have a large net effect on the overall system performance, thus requiring less mechanical movement of the compensator, assuming the compensator has enough mechanical resolution. The tilt of the focal plane is also a key compensator. It reduces the focus variation across the FOV that will not be compensated by tilting the secondary mirror, which primarily compensates astigmatism. With these two additional compensators added to the assembly, for any random as-built configuration, the tip and tilt of the secondary mirror and detector can be adjusted to remove the field constant astigmatism and image plane tilt to restore the optical performance to almost its nominal value.

The sensitivity analyses so far have not considered the irregularity of the optical surfaces. In a previous Letter, one of the optical surfaces of this system was measured interferometrically, and it was shown that the dominant figure error in the surface is astigmatism [5]. As a result, the overall system performance is going to be degraded by a field constant astigmatic aberration. In this case, the secondary mirror tilt can be used to introduce the opposite amount of field constant astigmatism present from the three fabricated optical surfaces. Ultimately, this property makes the entire optical system robust to both misalignment and fabrication induced figure errors.

Working with II–VI Infrared, the optical housing has been manufactured off-site based on the tolerances described in Table 1 and assembled at the University of Rochester. In Figs. 3(a)–3(c) the subassemblies of the three mirrors are shown for the primary, secondary, and tertiary. Within each subassembly, the three diamond turned raised pads and dowel pins can be seen that mate the subassembly to the optical housing. The secondary mirror subassembly, shown in Fig. 3(b), differs from the other two subassemblies, as it includes the aperture stop of the optical system. The elliptical knife edge rests above the secondary mirror and ensures the correct ray bundle enters the optical system.

The as-built optical system with the three subassemblies mated to the housing is shown in Fig. 3(d). With the use of the slip-fit steel dowel pins, the subassemblies readily mate to the faces of the optical housing. To minimize mounting distortion of the mirror components, the screws are tightened just enough to ensure that the

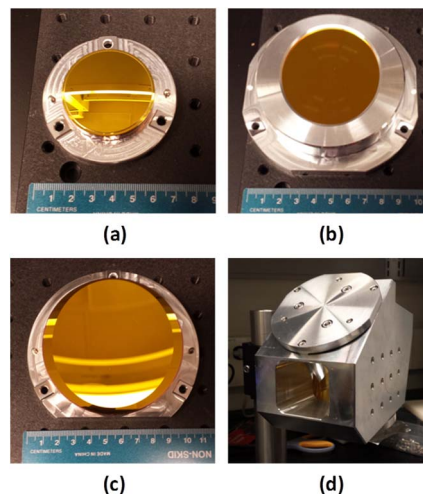


Fig. 3. As-built subassemblies for the (a) primary, (b) secondary, and (c) tertiary mirrors of the three mirror system that are to be mated to the optical housing. (d) Three mirror optical system with subassemblies mounted to the housing.

subassemblies are secure to the housing, as well as the mirrors secure to the adaptor plates.

The as-built full field performance of the assembled optical system is measured interferometrically with a Zygo 632.8 nm wavelength DynaFiz laser interferometer in a double-pass configuration. The interferometer is affixed with an $F/1.5$ transmission sphere, providing a spherical wavefront output that overfills the $F/1.9$ optical system. With this interferometer configuration, the optical system is oriented backward, that is, the output face of the optical system faces the interferometer. The point source focus of the interferometer is located at the image plane of the optical system by adjusting the position of the optical system that is mounted on a z -axis translation stage. When the point source is at the correct image plane location, the beam exiting the optical system is collimated. A 150 mm diameter, $\lambda/20$ high quality flat mirror is inserted at the input of the optical system so the wavefront is retro-reflected back toward the interferometer. The mirror is oversized relative to the entrance pupil diameter so that as the FOV is sampled, the beam does not vignette at the reference mirror surface. The FOV is sampled by mounting the optical system on both an x -axis and y -axis translation stage and moving the system laterally to different field points. At each field point, the mirror tip and tilt is adjusted to ensure the wavefront is retro-reflected back toward the interferometer.

The measured 3×3 grid of wavefronts across the $8 \text{ mm} \times 6 \text{ mm}$ image plane for the directly assembled system is shown in Fig. 4(a), where the RMSWFE at each field point is displayed inside the wavefront in micrometers. As can be seen in the structure of the wavefronts, the as-built system does suffer from field constant astigmatism oriented at zero degrees; however, the magnitude of the aberration is small and the RMSWFE throughout the FOV is less than 0.06λ at $10 \text{ }\mu\text{m}$, below the diffraction limit of 0.07λ .

The field constant astigmatism present in the directly assembled optical system results from a figure error of the as-fabricated surfaces and can be removed by tilting the secondary mirror. The required tilt of the secondary

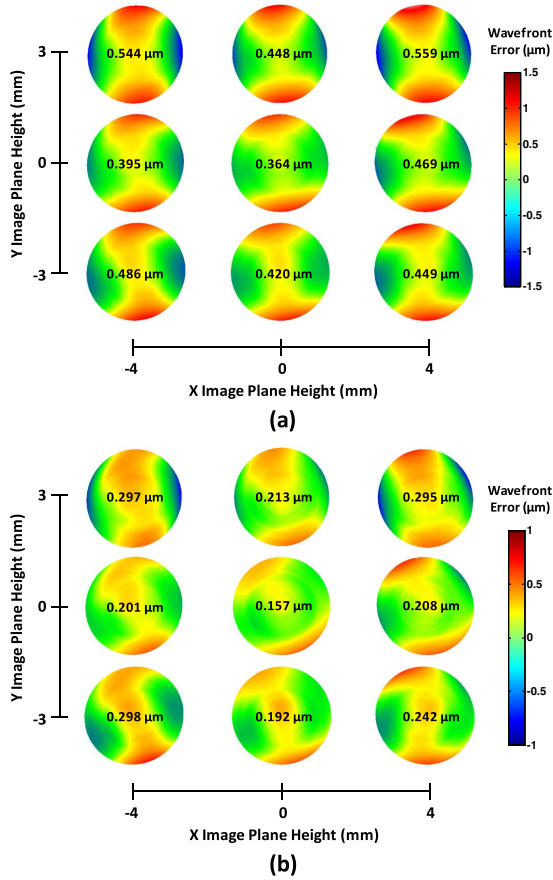


Fig. 4. (a) Measured wavefronts for a 3×3 grid of field points spanning an $8 \text{ mm} \times 6 \text{ mm}$ FOV for the directly assembled optical system and (b) with the secondary mirror tilted roughly 1 arc min with a $23 \text{ }\mu\text{m}$ shim. The RMSWFE in micrometers is displayed within the wavefront for each field.

mirror is dictated by the amount of field constant astigmatism present in the optical system. Using the on-axis field point as the evaluation point, the Zernike astigmatism ($Z5/6$) is measured for the as-built system and compared to its nominal value. The difference can be simulated in a commercial lens design software package, in this case CODE V, by adding the residual $Z5$ and $Z6$ astigmatism to the entrance pupil. Then in CODE V, the secondary mirror tilt can be re-optimized to remove the residual field constant astigmatism. Only the tilt in the YZ plane is allowed to vary because the tilt in the XZ plane is difficult to implement in the actual system where shims have to be used. From this simulation the optimum tilt is found to be -0.0175° , and it improves the overall performance so that it is near nominal with a maximum RMSWFE of 0.024λ at a wavelength of $10 \text{ }\mu\text{m}$. There is a trade-off for this improvement as the boresight of the optical system does change and the image shifts down $70 \text{ }\mu\text{m}$ in the y direction. For the detector with $25 \text{ }\mu\text{m}$ pixels, the secondary tilt results in a boresight error of three pixels. Based on the optical housing geometry, the



Fig. 5. Sample LWIR image from the optical system.

required shim is roughly $30 \text{ }\mu\text{m}$. As an example of this implementation, a $23 \text{ }\mu\text{m}$ shim at the secondary mirror has been implemented. Figure 4 shows the resulting performance for the measured 3×3 grid of wavefronts, and their corresponding RMSWFE at each field point is displayed inside the wavefront in microns. The maximum RMSWFE has improved by a factor of two to 0.03λ at a wavelength of $10 \text{ }\mu\text{m}$. Further improvement is still possible if the shim size is increased to $30 \text{ }\mu\text{m}$, and the mirror is shimmed out of plane to remove the residual field constant astigmatism oriented at 45° . However, even at this stage in the alignment, the optical system is well within the diffraction limit of 0.07λ at $10 \text{ }\mu\text{m}$ and would perform well if operated at $1 \text{ }\mu\text{m}$. As an example to demonstrate the image quality of the assembled optical system, Fig. 5 shows a sample image of the optical system affixed with the $8 \text{ mm} \times 6 \text{ mm}$, $25 \text{ }\mu\text{m}$ pixel pitch uncooled microbolometer detector.

In this Letter, the successful implementation of a free-form optical system has been demonstrated. The directly assembled optical system is diffraction limited throughout the FOV in the LWIR. If the system is actively aligned, the residual field constant astigmatism that results from a figure error of the mirror surfaces can be removed, further improving the optical performance. This work demonstrates a pathway for the use of these surfaces to systems operating at shorter wavelengths.

We acknowledge the Frank J. Horton Research Fellowship from the Laboratory for Laser Energetics, the II-VI Foundation, and the National Science Foundation (EECS-1002179) for supporting this research as well as Zygo and II-VI Infrared for their partnership in optical testing and assembly, respectively. We thank Synopsys Inc. for the student license of CODE V.

References

1. K. Fuerschbach, J. P. Rolland, and K. P. Thompson, *Opt. Express* **20**, 20139 (2012).
2. K. Fuerschbach, J. P. Rolland, and K. P. Thompson, *Opt. Express* **19**, 21919 (2011).
3. P. J. Smilie, B. S. Dutterer, J. L. Lineberger, M. A. Davies, and T. J. Suleski, *Opt. Eng.* **51**, 013006 (2012).
4. W. J. Smith, in *Modern Lens Design* (McGraw-Hill, 2005), pp. 582–584.
5. K. Fuerschbach, K. P. Thompson, and J. P. Rolland, *Opt. Lett.* **39**, 18 (2014).